18TH WORLD CONFERENCE ON EARTHQUAKE ENGINEERING
WCEE2024
MILAN

MILAN, ITALY
30TH JUNE - 5TH JULY 2024

www.wcee2024.it

CORRELATION MODELS FOR FILTERED INCREMENTAL VELOCITY WITH SPECTRAL ACCELERATION AND SIGNIFICANT DURATION

S. Aristeidou[1], D. Shahnazaryan[2] & G. J. O'Reilly[2]

[1]Centre for Training and Research on Reduction of Seismic Risk (ROSE Centre), Scuola Universitaria Superiore IUSS Pavia, Italy, savvinos.aristeidou@iusspavia.it

[2]Centre for Training and Research on Reduction of Seismic Risk (ROSE Centre), Scuola Universitaria Superiore IUSS Pavia, Italy

Abstract: *A recently proposed intensity measure (IM), namely filtered incremental velocity, FIV3, was shown to have strong potential in predicting the seismic collapse of structures. A ground motion model (GMM) was also developed recently to predict the probability distribution of this period-dependent IM, given a set of seismological and filtering parameters. Nonetheless, there is still a need for correlation models if one wants to perform seismic hazard analysis and ground motion selection using FIV3 via, say, the conditional spectrum method. Examining its correlation with other IMs, such as spectral acceleration, Sa, and significant duration, Ds_{595}, will also enable a more generalised selection and scaling of ground motions via the generalised conditional intensity measure (GCIM) method. The motivation to use these IMs is the high predictive power they exhibit not only over the structural collapse limits, but also throughout the whole non-linear response of structures. A generalised ground motion model (GGMM) estimating all the aforementioned IMs, using machine-learning techniques, based on the NGA-West2 database was utilised to calculate the correlations between the residuals. Correlations were calculated for intra- and inter- event residuals, but only the ones for total residuals are presented here. To facilitate the usage of these correlation coefficients, predictive models of the empirical data were developed using again machine-learning-based techniques, namely artificial neural networks (ANNs). The period range of applicability of these correlation models spans from 0.01 s to 5 s, for Sa and from 0.1 s to 4 s for FIV3. It was found that FIV3 is strongly correlated with Sa(~1s) and itself across all periods, and has a weak negative correlation with duration at short periods and near-zero correlation for longer periods.*

1. Introduction

The earthquake-induced ground motion severity can be quantified via a plethora of proxies describing the amplitude, frequency content and duration of ground shaking, termed as intensity measures (IMs). Traditionally, the ground motion amplitude and frequency content are explicitly considered through the examination of acceleration-based response spectrum quantities. However, other type of IMs, like duration or filtered incremental velocity, *FIV3*, have received less attention despite being efficient predictors of structural response (Bojórquez et al., 2012). These 'secondary' features of ground motion shaking (i.e., duration, energy content, velocity-based IMs etc.) are assumed to be implicitly accounted for by limiting the causal parameters (e.g., magnitude, source-to-site) of the selected ground motion record set (Bommer and Acevedo, 2004; ASCE, 2017; Spillatura et al., 2021).

Regarding the importance of duration, Hancock and Bommer (2006) summarised how different conclusions have been drawn in the literature, depending on the structural demand parameters considered in each study. A few studies that considered only peak structural deformations (Sarieddine and Lin, 2013) found that duration has little effect. Meanwhile, most other studies (Iervolino et al., 2006; Oyarzo-Vera and Chouw, 2008; Raghunandan and Liel, 2013; Chandramohan et al., 2016; Gentile and Galasso, 2021) found that, while

duration does not influence the peak deformations, it does influence the cumulative engineering demand parameters, and therefore the damage due to cumulative effects. Nevertheless, it is always important to consider the correlation of duration with *Sa* when examining the effects of duration on structural response.

Regarding the importance of *FIV3*, some recent studies highlighted the value of this IM in estimating seismic collapse in buildings and bridges (Dávalos and Miranda, 2019; Dávalos and Miranda, 2020; Aristeidou and O'Reilly, 2023). There is already one empirical ground motion model (GMM) for the estimation of this IM (Dávalos et al., 2020). It is envisaged that when used with *Sa* (or average spectral acceleration, Sa_{avg}) and even 5–95% significant duration, Ds_{595}, in a generalised conditional intensity measure (GCIM) ground motion selection procedure (Bradley, 2010), one can enjoy high predictive power, not only in collapse estimates, but throughout the non-linear response of structures. Following this same line of thinking, there is an increased interest to select ground motion records based on multiple ground motion features for non-linear response history analysis (Katsanos et al., 2010). This reduces the record-to-record variability, increases the efficiency of the prediction, and better represents the seismic hazard conditions in the analysis as part of the overall performance-based earthquake engineering framework (Sousa et al., 2016).

With more advanced record selection methods like the GCIM, it became possible to explicitly consider several IMs. To use this method, GMMs and correlation models are needed for each of the IMs utilised. The GMM provides the marginal, or unconditional, distribution of an IM given specific causal parameters (Baker et al., 2021). To obtain conditional distributions of an IM with other relevant IMs, the correlation between them is needed. To date, there are no available correlation models of inter-spectral *FIV3* values and *FIV3* with other IMs. Therefore, in this paper the following correlation are proposed: *FIV3*-*FIV3*; *FIV3*-*Sa*; *FIV3*-Ds_{595}; *Sa*-*Sa*; *Sa*-Ds_{595}. Additionally, these correlations can find use in particular performance-based assessments, where it is often required to estimate the joint probability of occurrence of the IMs through a vector-PSHA (Bazzurro and Cornell, 2002).

This paper explores the use of machine learning-based techniques, namely artificial neural network (ANN), for the predictive models of correlations among the IMs discussed above, instead of the traditional way of identifying functional forms, which in some cases might deviate from empirical values in their estimations. Firstly, the IMs are described in more detail, describing their computation, along with a brief description of the adopted GMM and strong motion database. Secondly, the methodology for computing the correlation coefficients is outlined and the architecture of ANN models is outlined. Finally, the quantified empirical correlations are appraised and the comparisons with the fitted ANN models and other existing models are discussed.

2. Intensity measures

The correlations between the following IMs were investigated in this study:

- *Sa(T)*: 5%-damped spectral acceleration at a vibration period, *T*. The *RotD50* horizontal component definition (Boore, 2010) was adopted.
- Ds_{595}: 5-95% significant duration, defined as the time interval over which 5% to 95% of the integral $\int_0^{t_{max}}[a(t)]^2dt$ is accumulated (Trifunac and Brady, 1975), as per Eq. (1).
- *FIV3*: filtered incremental velocity, defined by Dávalos and Miranda (2019) and summarised in Eq. (3)

Even though there are many ways to describe the duration of a strong ground motion (Bommer and Martínez-Pereira, 1999), the two most common definitions are bracketed duration and significant duration (Afshari and Stewart, 2016). The scope herein is limited to the significant duration, since it is often the preferred definition used in the literature (Chandramohan et al., 2016). It is defined as follows:

$$Ds_{xy} = t_y - t_x \tag{1}$$

$$x = \frac{100\%}{I_a}\int_0^{t_x}[a(t)]^2dt \tag{2}$$

where t_x and t_y are the time stamps on a Husid plot (Husid, 1969) at which *x* and *y* percent of the total Arias intensity, I_a, occurs (as defined in Eq. (2) for *x* and similarly for *y*). The most common values of *x* and *y* adopted in the literature are {*x*, *y*} = {5%,75%} and {*x*, *y*} = {5%, 95%}, subsequently referred to as D_{S575} and D_{S595}, respectively, where only Ds_{595} will be discussed herein.

Dávalos and Miranda (2019) proposed *FIV3* as a novel IM that showed promising results regarding its efficiency and sufficiency on characterising the collapse performance of buildings. It is briefly summarised mathematically as follows:

$$FIV3 = \max\left\{V_{s,max1} + V_{s,max2} + V_{s,max3}, \left|V_{s,min1} + V_{s,min2} + V_{s,min3}\right|\right\} \quad (3)$$

$$V_s(t) = \left\{\int_t^{t+\propto\cdot T} \ddot{u}_{gf}(\tau)d\tau, \quad \forall t < t_{end} - \propto\cdot T\right\} \quad (4)$$

where $V_s(t)$ is a series of incremental velocities, *IVs*, computed using time segments with duration $\alpha \cdot T$ via Eq. (4), $V_{s,max1}$, $V_{s,max2}$, and $V_{s,max3}$, are the three local maxima *IVs* in $V_s(t)$ and $V_{s,min1}$, $V_{s,min2}$, and $V_{s,min3}$, are the three local minima *IVs* in $V_s(t)$, T, corresponds to the period of vibration of interest, t_{end} corresponds to the last instant of time of the acceleration time series, and $\ddot{u}_{gf}$ corresponds to the filtered acceleration time series using a second-order Butterworth low-pass filter with a cut-off frequency, f_c, equal to $\beta \cdot f$, where β is a scalar input that controls the f_c/f ratio. The α and β input parameters required to calculate Eq. (3) were chosen as 0.7 and $1/f$ (or T), respectively, as these were the parameters chosen in the original study (Dávalos et al., 2020).

3. Estimation of residuals

To estimate the correlations between the aforementioned IMs, two important inputs are needed: a ground motion database and a GMM to predict the expected shaking intensity for these same rupture parameters. For each ground motion record in the database adopted, the residuals are computed as the difference between the actual observation (i.e., the ground motion record's value of IM) and the predicted median value from the GMM; as illustrated in Figure 1 for two values of a spectral IM. These residuals are computed for all IM definitions and the correlation between these residuals is then quantified and modelled later in the paper.

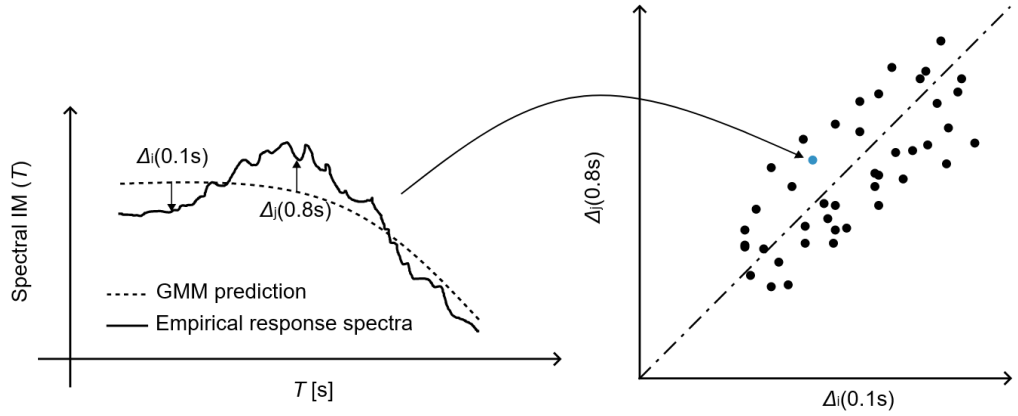

Figure 1. Schematic representation of correlation between total residuals, Δ. (Left) Predicted and empirical response spectrum for a single record and (Right) residuals of the same IM from a set of records

Regarding the GMM adopted in this study, the estimated IM distributions were obtained from a single generalised ground motion model (GGMM) applicable for active shallow crustal tectonic regions. This model is presented in O'Reilly et al. (2024), and not discussed in detail here. It was developed using the strong motion database from NGA-West2 (Ancheta et al., 2013) using an ANN framework. The appliable period range of the GGMM for *Sa* is 0.01 s – 5 s, while for *FIV3* is 0.1 s – 4 s. Although other GMMs may have been used, only one was considered here to compute the residuals with reference to these predictions. Studies such as (Baker and Bradley, 2017) have examined the impact of considering different GMMs and strong motion databases when computing residuals and noted that while there is some difference, it is not considered to have a significant impact on the computed correlation coefficients. Therefore, it was deemed acceptable to use a single GGMM for all IMs examined herein. The ground motion records used are the same as those used to develop the GGMM from the NGA-West2 database (Ancheta et al., 2013), and have with the same filtering criteria as described in O'Reilly et al. (2024), amounting to 4131 ground motion records from 96 earthquakes. Therefore, the inter-event, intra-event and total residuals obtained from the GGMM were passed on to this study to compute the empirical cross-correlation of the IM residuals.

For further cross-validation of the GGMM, Figure 2 depicts the empirical distributions of the normalised inter- and intra-event residuals for Ds_{595}, $Sa(T=1s)$ and $FIV3(T=1s)$. They are compared with the theoretical standard normal distribution and the Kolmogorov–Smirnov (KS) goodness-of-fit bounds at 5% significance level. The compatibility of the GGMM with this dataset is demonstrated by the observation that both inter- and intra-event empirical distributions lie within the KS goodness-of-fit bounds. Figure 2 depicts just three IMs but similar results were obtained for the other IMs considered.

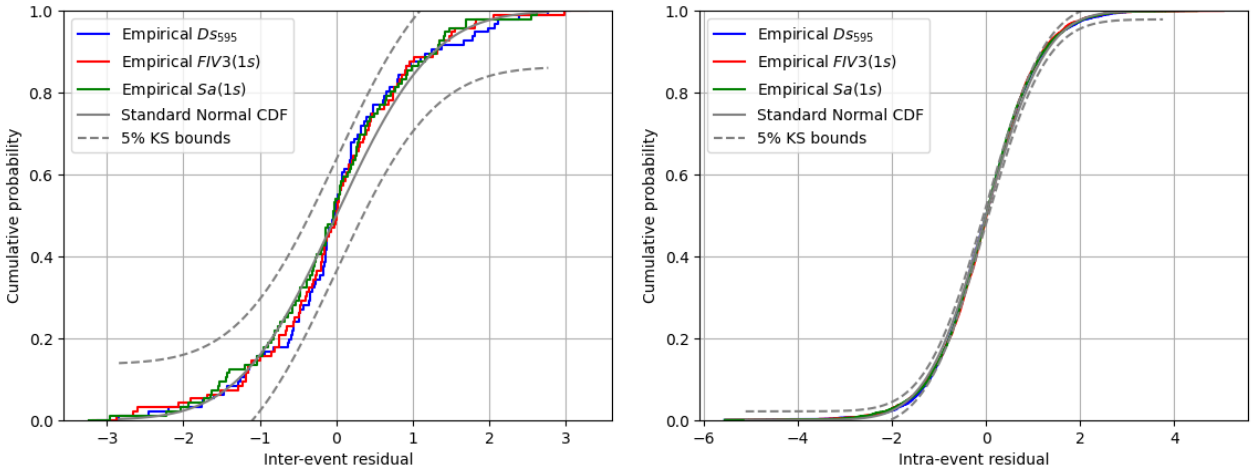

Figure 2. Empirical cumulative distribution of the (a) normalised inter-event; and (b) normalised intra-event residuals obtained using the GGMM. Comparison with the theoretical standard normal cumulative distribution and the KS bounds

4. Methodology

The general form of the generalised ground motion model is given as:

$$\log_{10} IM_i = f_i(\boldsymbol{X}, \boldsymbol{\theta}) + \delta b_i \tau_i + \delta w_i \varphi_i \tag{5}$$

where $log_{10}(IM_i)$ is logarithm with base 10 of the ith IM; $f_i(\boldsymbol{X}, \boldsymbol{\theta}) = \mu_{\log_{10} IM_i|\boldsymbol{X},\theta}$ is the predicted mean output from the ANN model, taking as input a set of GM causal parameters (M_w, R_{rup}, etc.), denoted as $\boldsymbol{X}$; $\boldsymbol{\theta}$ are the 'calibrated coefficients' of the ANN model (i.e., synaptic weights and biases); δb_i and δw_i are the normalised inter- and intra-event residuals of IM_i, respectively; τ_i and φ_i are the inter- and intra-event logarithmic standard deviations. The total normalised residual, δ_i, and total standard deviation, σ_i, can be expressed as the sum of inter- and intra-event residuals as:

$$\delta_i \sigma_i = \delta b_i \tau_i + \delta w_i \varphi_i \tag{6}$$

Combining Eqs. (5) and (6), and rearranging, the total normalised residual for a specific ground motion g, $\delta_{i,g}$, can be thought of as the number of standard deviations that the empirical IM is above the predicted mean value from the GMM, as illustrated in Figure 1 and formally described as:

$$\delta_{i,g} = \frac{\log_{10} IM_{i,g} - \mu_{\log_{10} IM_i|\boldsymbol{X},\boldsymbol{\theta}}}{\sigma_i} \tag{7}$$

It can be seen that $\log_{10} IM_{i,g}$ and $\delta_{i,g}$ exhibit a linear relationship in Eq. (7), therefore by extension the correlation between two IMs, for given GM causal parameters $\boldsymbol{X}$, is equal to the correlation between the normalised residuals, which in mathematical form translates to:

$$\rho_{\log_{10} IM_i|\boldsymbol{X},\boldsymbol{\theta},\ \log_{10} IM_j|\boldsymbol{X},\boldsymbol{\theta}} = \rho_{\delta_i,\ \delta_j} \tag{8}$$

Herein, for the sake of brevity, the correlation between two IMs will be simply referred to as $\rho_{\log_{10} IM_i, IM_j}$, where the conditioning on the GM causal parameters is implied, but is generally taken as independent.

Since δb_i and δw_i are assumed to be independent in the recently developed GGMM used for this study (Abrahamson et al., 2008), the correlations of inter- and intra-event residuals between different IMs can be estimated using the Pearson product-moment correlation coefficient formula:

$$\rho_{x,y} = \frac{\sum_n[(x-\bar{x})(y-\bar{y})]}{\sqrt{\sum_n[(x-\bar{x})^2]\sum_n[(y-\bar{y})^2]}} \tag{9}$$

where x and y are generic variables, corresponding to δb_i and δb_j for inter-event correlation for IMs i and j, and to δw_i and δw_j for intra-event correlation in this application; $\bar{x}$ and $\bar{y}$ are the sample means and Σ_n is the summation over all n ground motion records. Therefore, Eq. (9) was used to compute the $\rho_{\delta b_i,\delta b_j}$ and $\rho_{\delta w_i,\delta w_j}$ correlations separately. From the definition of correlation coefficient, the correlation between total residuals can be estimated from the inter- and intra-event correlations as follows:

$$\rho_{\delta_i,\delta_j} = \frac{\rho_{\delta b_i,\delta b_j}\tau_i\tau_j + \rho_{\delta w_i,\delta w_j}\varphi_i\varphi_j}{\sigma_i\sigma_j} \tag{10}$$

Baker and Bradley (2017) studied the dependence of IM correlations on causal parameters such as magnitude, distance and time-averaged shear wave velocity to 30m depth, $V_{s,30}$. They found no systematic variation of these correlations with any of these GM causal parameters and corroborated the typical assumption that IM correlations are independent of these parameters (Huang and Galasso, 2019; Tarbali et al., 2023). To account for the GMM uncertainty in the computed correlation coefficient, more than one GMM for active shallow crustal tectonic regions could be used with a logic tree; however, this was not applied here and only a single GMM was used. Additionally, only the point estimate of the correlation coefficient is utilised here, and not its uncertainty due to the finite number of recordings used in its determination.

5. Artificial neural network models

The results of the empirical correlations calculated were then used to fit predictive models. Traditionally these regression models (or predictive equations) are analytical functions with no strong physical basis and are developed simply to fit the observed data. Because of this lack of physical basis, which an analytical GMM may have based on knowledge of wave propagation, these analytical models might deviate significantly from the empirical correlation data in some places. To address this potential for poor fitting due to analytical functional form constraints, machine learning techniques were employed here. In particular, ANN (McCulloch and Pitts, 1943) was used to fit the data, eliminating the need to find suitable functional forms and keeps the misfit between observed and predicted data to a minimum. To the best of the authors' knowledge, this technique has not been used to date for fitting predictive correlation models. To facilitate these models' usage and implementation for users, they will be made publicly available via online repositories such as GitHub.

To adopt this technique, an ANN architecture first needs to be set up and the optimal hyperparameters for each model need to be chosen. A schematic representation of the network is illustrated in Figure 3 for the example case of *Sa-FIV3* correlation model, where the weights, W, and biases, b, of activation function are also depicted. Meanwhile the chosen hyperparameters for each model are listed in Table 1. Two hidden layers were required in most of the models to represent well the trends of the empirical data, with a high number of neurons per layer. Softmax, linear and sigmoid activation functions were employed, as they were found to be the optimal for the problem at hand. Also, a large number of epochs was chosen, as the goal here was to have the model predict values that are as close to the empirical ones as possible. In other words, overfitting here is desirable. Regarding the batch size, a small number was chosen in these models, since the training dataset is exceptionally small. The mean squared error (MSE) was selected as the loss function metric, which was minimised by the adaptive moment (ADAM) estimation algorithm (Kingma and Ba, 2014).

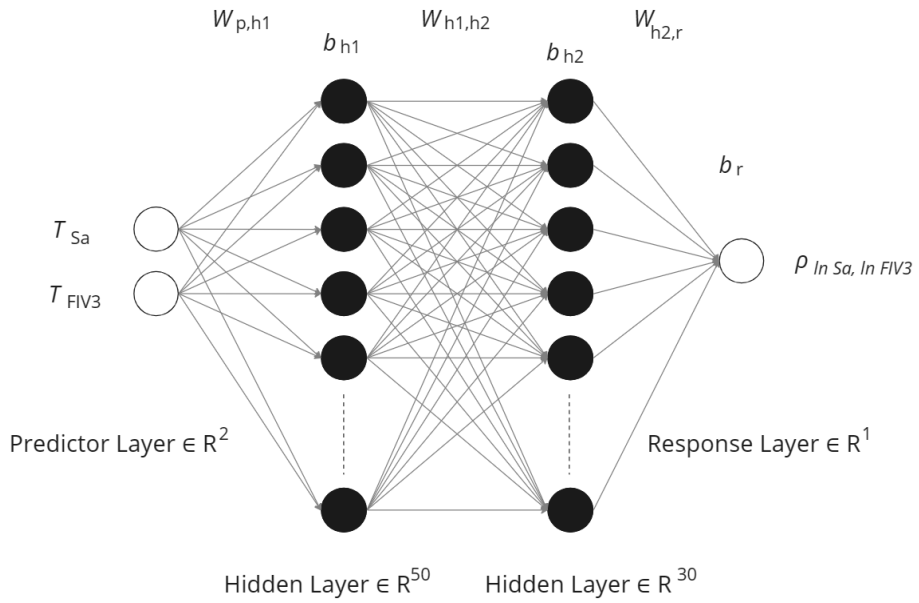

Figure 3. Schematic representation of ANN architecture for the case of Sa-FIV3 correlation model

Table 1. Key hyperparameters and general architecture of the adopted ANN correlation model

Correlation model	***Sa-FIV3***	***Sa-Sa***	***FIV3-FIV3***	***FIV3-Ds$_{595}$***	***Sa-Ds$_{595}$***
Number of hidden layers	2	2	1	2	2
Activation functions	linear → softmax → linear → linear	linear → sigmoid → sigmoid → linear	linear → softmax → linear	linear → softmax → linear → linear	linear → softmax → softmax → linear
Number of neurons per hidden layer	50 & 30	60 & 30	300	30 & 30	60 & 40
Epochs	700	1000	3000	400	1500
Batch size	16	16	16	4	4

6. Results

6.1. Empirical results and model estimates

Past studies, such as Bradley (2011b), for example, have shown that the distribution of the correlation coefficient, which includes both finite sample size and GMM uncertainty, can be represented by the normal distribution. In this study, only results for the mean correlation coefficients are presented.

The most common correlation studied here is that of *Sa-Sa*, since studies such as Baker and Jayaram (2008) have investigated this and proposed existing models. This correlation model will be discussed further in the next section with reference to existing models. Instead, Figure 4 first presents the observed empirical correlations between *Sa* and *FIV3*, where the correlation values range from 0.32 to 0.96. Since these IMs are period-dependent in their definition, the correlation coefficient is plotted as a surface for all combinations of period values. These results indicate that *FIV3* of most periods are highly correlated with *Sa(1s)*, which is the IM recommended by HAZUS (2003) to be used for seismic assessment of bridges in the US. Also shown in Figure 4 are the corresponding predictions by the proposed ANN model, it can be seen that the proposed correlation model can capture the empirical data very well.

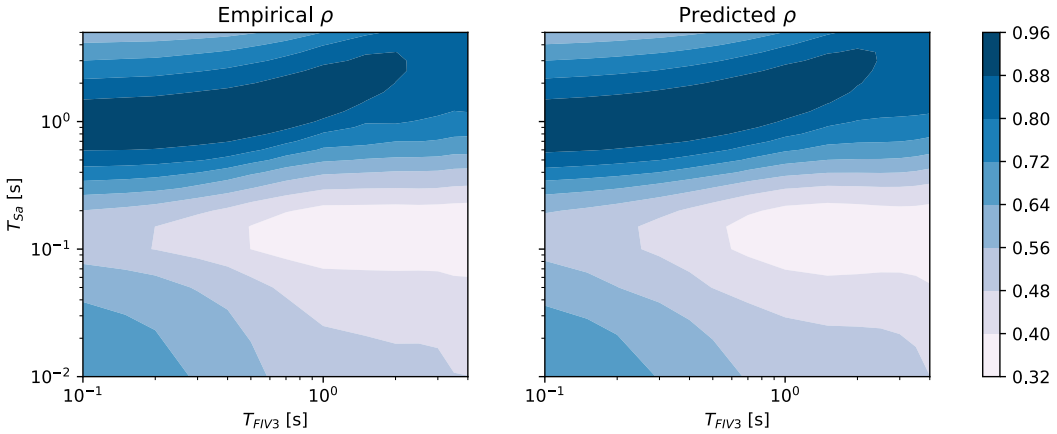

Figure 4. Empirical and corresponding predicted correlation coefficients between Sa and FIV3

Figure 5 illustrates the empirical and predicted correlation coefficients between Ds_{595} and *FIV3*. Firstly, it can be observed that the correlation between these two IMs is negative, with values ranging from -0.275 for the lowest period *FIV3* to about -0.08 for the highest period *FIV3*. The trend is monotonically increasing and plateauing after an *FIV3* of period 2 s. These results suggest that a ground motion with a higher-than-expected *FIV3* will, on average, have a lower than usual significant duration. This is possibly because the ground motion has released all of its energy within a few strong velocity pulses rather than over a long duration. The trend is very similar to the correlation between Sa and Ds_{595}. All in all, the empirical results suggest that *FIV3* is more correlated with *Sa* than Ds_{595}.

Regarding inter-IM correlation, Figure 6 shows the correlations of FIV3 to itself at different periods, with correlation coefficients ranging from 0.84 to 1, which is suggesting that *FIV3* is strongly correlated to itself. Figure *7* illustrates this same data slightly differently whereby specific slices of Figure 6 are shown. Also shown are the *Sa-Sa* correlations that will be discussed in the next section, where this relative comparison illustrates that *FIV3* is much more correlated to itself across different periods than *Sa*. This signifies that *FIV3* can be treated as almost a period-independent IM, in a similar way that peak ground acceleration has been used traditionally, but not entirely.

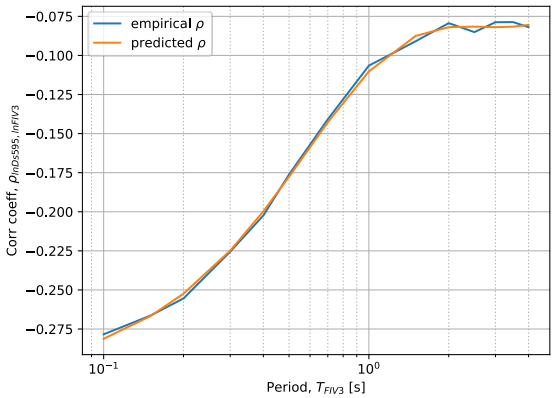

Figure 5. Empirical and corresponding predicted correlation coefficients between Ds_{595} and FIV3

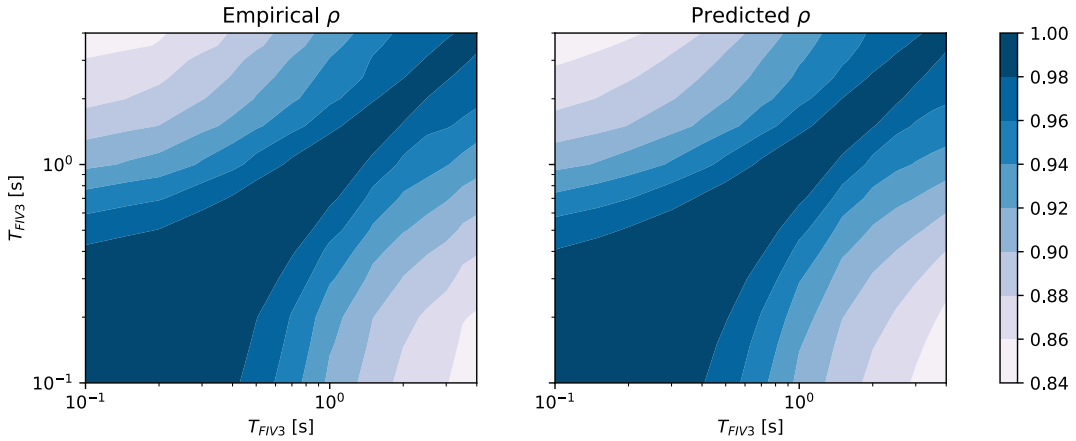

Figure 6. Empirical and corresponding predicted correlation coefficients between FIV3 of different periods

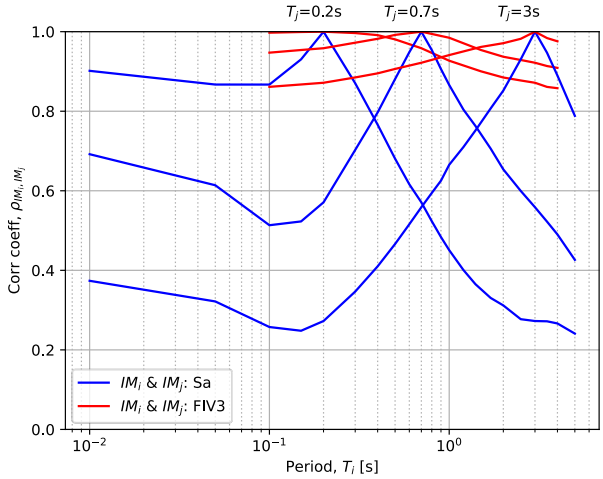

Figure 7. Empirical correlation coefficients between Sa-Sa and FIV3-FIV3 for three values of T_j

6.2. Comparison with existing correlation models

Two out of the five total IM cross-correlation models developed within this study are well documented in literature. Therefore, two well-established models were selected for comparison. For the case of *Sa-Sa* correlations, the work of Baker and Jayaram (2008) is referred to, where for the case of *Sa-Ds*$_{595}$*, the work of* Bradley (2011a) was used. To the best of the authors' knowledge, there are no available correlation models of *FIV3* with any other IM or with itself, which is a novelty of this study.

From Figure 8 it can be observed that the correlations predicted by the Baker and Jayaram (2008) model somewhat deviate from the empirical ones computed here. This may be due to several factors, the first of which is the different in ground motion databases used, where that study used the NGA-West1 database with an approximately 2500 recordings available at moderate periods, whereas this study utilised the NGA-West2 database with 4131 records. The second factor relates to the GMM model from which the residuals were computed, which differed to that adopted here. Lastly, the plot shows the analytical function fitting, hence the expected errors involved in functional form identification can also be anticipated. Meanwhile, the correlations predicted by the ANN model developed in this study are almost identical to the empirical data. This is seen through the general pattern of the correlation model, which closely follows that of the empirical data. This was very encouraging to see since it illustrates the utility of ANN models in this regard, which have yet to be employed for this purpose.

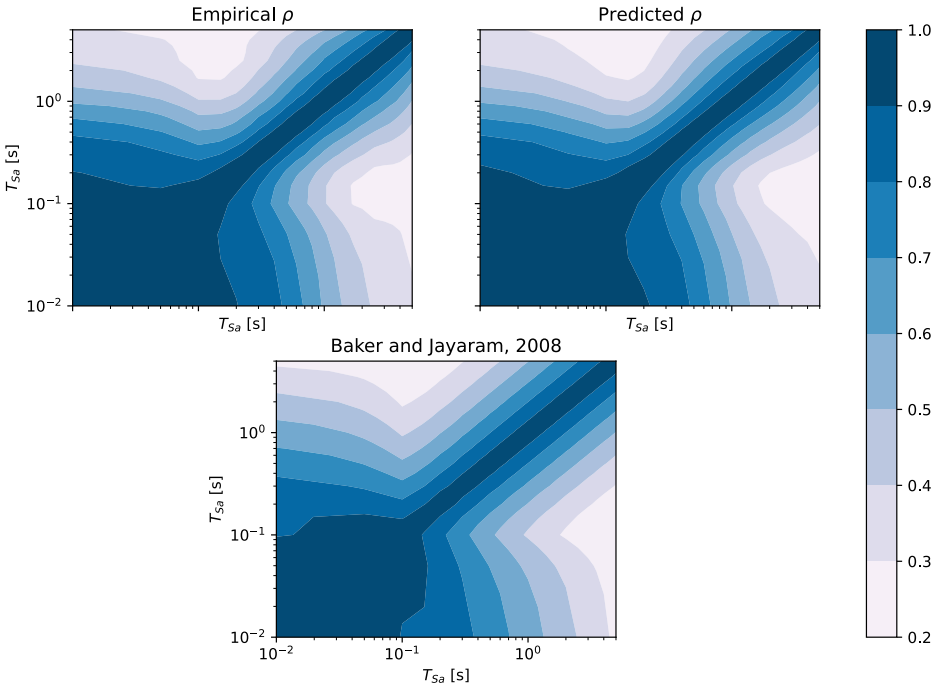

Figure 8. Empirical and predicted Sa-Sa correlation of the ANN and Baker and Jayaram (2008) models

It can be generally observed that short-period spectral accelerations exhibit the strongest correlations, which is well-captured in both models. The precision of the predictive ANN model and the difference from the Baker and Jayaram (2008) model can be better appreciated in Figure 9, where the correlation coefficients are plotted between *Sa(T_i)* and *Sa(T_j)* for four values of T_j. It can be seen that the proposed ANNN model matches the empirical data very well across all periods of vibration. The model of Baker and Jayaram (2008) matches quite well when T_i is close to T_j. However, when the inter-period distance increased, the model begins to underpredict the correlation. The impact of this underprediction on ground motion selection via conditional spectrum (Baker, 2011) would be that the variance around the target mean would be slightly higher, meaning that the selected ground motions would be more disperse than they perhaps should be. For structures where this spectral content at periods away from the conditioning period is relevant, it may result in an overprediction of structural demands.

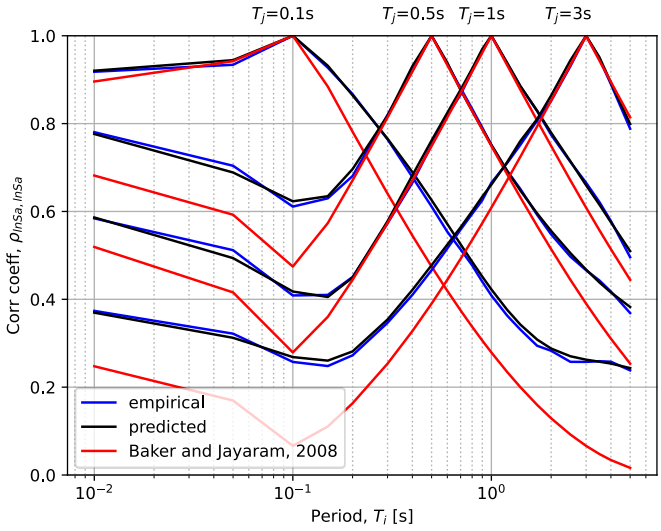

Figure 9. Correlation coefficients between Sa(T_i) and Sa(T_j) for four values of T_j

In the case of significant duration, Figure *10* shows that the empirical correlation with *Sa* increases (i.e., takes less negative values) with increasing vibration period. The increase is monotonically increasing, except for the

period range between 0.1-0.3 s, where the slope is momentarily negative. This is caused by a sudden small increase in correlation for *Sa(0.1s)*. Same observations were also noticed by previous studies (Bradley, 2011a; Baker and Bradley, 2017), but may be a consequence of the available data rather than an underlying physical feature. Nevertheless, this behaviour is regressed by a smoothed, monotonically increasing, curve. Regarding the comparison with the Bradley (2011a) model, the trend is very similar, but the correlations computed herein are shifted downwards by about 0.1 across the whole range of *Sa* periods. This is likely due to the difference in the ground motion database used (NGA-West1 versus NGA-West2) and the different GMMs employed. Also, the total number of ground motions utilised in that study was 1842. The fact that correlation between Ds_{595} and high-period IMs (i.e., *Sa*(*T*>2s) and *FIV3*(*T*>1s)) is relatively small, suggests that the majority of their dependence is captured by the median GMM of these IMs. Generally, duration exhibits negative correlation with low-period IMs.

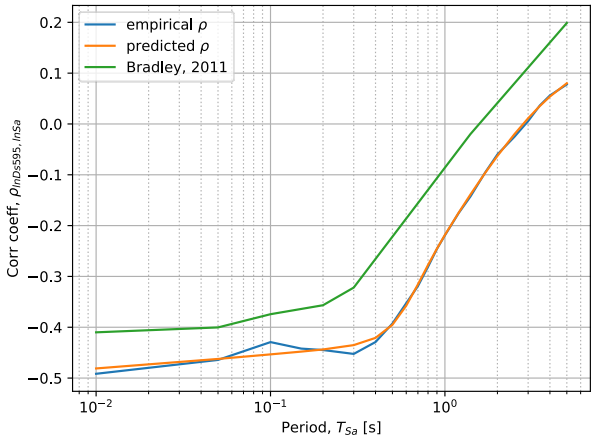

Figure 10. *Empirical and predicted Sa-Ds_{595} correlation of the ANN and Bradley (2011a)* models

7. Conclusions

This paper presented the empirical correlations for a given set of ground motion causal parameters, between three different types of IMs, namely *FIV3*, *Sa* and Ds_{595}. In total five correlation models based on a novel approach via artificial neural networks (ANN) were proposed, and it was shown how they fit the empirical data very well. Two well-established correlation models from the literature were also compared with the ANN-based correlation models proposed here. Based on this, the following conclusions can be drawn out from this research:

- The *FIV3* presented relatively strong correlation with *Sa*, especially in the range of *Sa*(*T*=0.6s) to *Sa*(*T*=3s), which indicates that *FIV3* is best correlated with moderate-period IMs, and weakly correlated with low-period IMs;
- The correlation between significant duration Ds_{595} and *FIV3* showed the same trend as that of Ds_{595} and *Sa* but with a slightly weaker correlation (i.e., taking values closer to 0);
- It was found that *FIV3* is strongly correlated with itself, with the correlation values not dropping below 0.84, essentially making this IM almost period-independent, which could be useful for more general and regional studies;
- The empirical results obtained in this study present some small differences when compared to existing models, attributed mainly to the differences in the filtered database and GMM used.
- The proposed predictive ANN models estimate the empirical data with high precision, while facilitating a seamless application since the model will be readily available online.

8. Acknowledgments

The work presented in this paper has been developed within the framework of the project “Dipartimenti di Eccellenza 2023-2027”, funded by the Italian Ministry of Education, University and Research at IUSS Pavia.

9. References

Abrahamson N., Atkinson G., Boore D., Bozorgnia Y., Campbell K., Chiou B., Idriss I.M., Silva W., Youngs

R. (2008). Comparisons of the NGA Ground-Motion Relations, *Earthquake Spectra*, 24(1): 45–66.

Afshari K., Stewart J.P. (2016). Physically parameterized prediction equations for significant duration in active crustal regions, *Earthquake Spectra*, 32(4): 2057–2081.

Ancheta T., Darragh R., Stewart J., Seyhan E., Silva W., Chiou B., Wooddell K., Graves R., Kottke A., Boore D., Kishida T., Donahue J. (2013). PEER NGA-West2 Database, Technical Report PEER 2013/03,

Aristeidou S., O'Reilly G.J. (2023). Exploring the use of orientation-independent inelastic spectral displacements in the seismic assessment of bridges, *Under Review*,: 1–21.

ASCE (2017). *Minimum design loads for buildings and other structures*, ASCE 7-16. American Society of Civil Engineers.

Baker J., Bradley B., Stafford P. (2021). *Seismic Hazard and Risk Analysis*, 1st Ed., Cambridge University Press.

Baker J.W. (2011). Conditional Mean Spectrum: Tool for Ground-Motion Selection, *Journal of Structural Engineering*, 137(3): 322–331.

Baker J.W., Bradley B.A. (2017). Intensity Measure Correlations Observed in the NGA-West2 Database, and Dependence of Correlations on Rupture and Site Parameters, *Earthquake Spectra*, 33(1): 145–156.

Baker J.W., Jayaram N. (2008). Correlation of spectral acceleration values from NGA ground motion models, *Earthquake Spectra*, 24(1): 299–317.

Bazzurro P., Cornell C.A. (2002). Vector-valued Probabilistic Seismic Hazard Analysis (VPSHA), *Proceedings of the 7th US National Conference on Earthquake Engineering*,.

Bojórquez E., Iervolino I., Reyes-Salazar A., Ruiz S.E. (2012). Comparing vector-valued intensity measures for fragility analysis of steel frames in the case of narrow-band ground motions, *Engineering Structures*, 45: 472–480.

Bommer J.J., Acevedo A.B. (2004). The use of real accelerograms as input to dynamic analysis, *Journal of Earthquake Engineering*, 8(sup001): 43–91.

Bommer J.J., Martínez-Pereira A. (1999). Tha effective duration of earthquake strong motion, *Journal of Earthquake Engineering*, 3(2): 127–172.

Bommer J.J., Stafford P.J., Alarcon J.E. (2009). Empirical Equations for the Prediction of the Significant, Bracketed, and Uniform Duration of Earthquake Ground Motion, *Bulletin of the Seismological Society of America*, 99(6): 3217–3233.

Boore D.M. (2010). Orientation-independent, nongeometric-mean measures of seismic intensity from two horizontal components of motion, *Bulletin of the Seismological Society of America*, 100(4): 1830–1835.

Bradley B.A. (2010). A generalized conditional intensity measure approach and holistic ground-motion selection, *Earthquake Engineering and Structural Dynamics*, 39(12): 1321–1342.

Bradley B.A. (2011a). Correlation of significant duration with amplitude and cumulative intensity measures and its use in ground motion selection, *Journal of Earthquake Engineering*, 15(6): 809–832.

Bradley B.A. (2011b). Empirical equations for the prediction of displacement spectrum intensity and its correlation with other intensity measures, *Soil Dynamics and Earthquake Engineering*, 31(8): 1182–1191.

Chandramohan R., Baker J.W., Deierlein G.G. (2016). Quantifying the influence of ground motion duration on structural collapse capacity using spectrally equivalent records, *Earthquake Spectra*, 32(2): 927–950.

Dávalos H., Heresi P., Miranda E. (2020). A ground motion prediction equation for filtered incremental velocity, FIV3, *Soil Dynamics and Earthquake Engineering*, 139: 106346.

Dávalos H., Miranda E. (2020). Evaluation of FIV3 as an Intensity Measure for Collapse Estimation of Moment-Resisting Frame Buildings, *Journal of Structural Engineering*, 146(10): 1–14.

Dávalos H., Miranda E. (2019). Filtered incremental velocity: A novel approach in intensity measures for seismic collapse estimation, *Earthquake Engineering and Structural Dynamics*, 48(12): 1384–1405.

Gentile R., Galasso C. (2021). Hysteretic energy-based state-dependent fragility for ground-motion sequences, *Earthquake Engineering & Structural Dynamics*, 50(4): 1187–1203.

Hancock J., Bommer J.J. (2006). A State-of-Knowledge Review of the Influence of Strong-Motion Duration on Structural Damage, *Earthquake Spectra*, 22(3): 827–845.

HAZUS (2003). *Multi-hazard loss estimation methodology - earthquake model,* Washington, DC, USA.

Huang C., Galasso C. (2019). Ground-motion intensity measure correlations observed in Italian strong-motion records, *Earthquake Engineering & Structural Dynamics*, 48(15): 1634–1660.

Husid R. (1969). Características de terremotos. Análisis general, *Revista IDIEM*, 8(1): 21–42.

Iervolino I., Manfredi G., Cosenza E. (2006). Ground motion duration effects on nonlinear seismic response, *Earthquake Engineering and Structural Dynamics*, 35(1): 21–38.

Katsanos E.I., Sextos A.G., Manolis G.D. (2010). Selection of earthquake ground motion records: A state-of-the-art review from a structural engineering perspective, *Soil Dynamics and Earthquake Engineering*, 30(4): 157–169.

Kingma D.P., Ba J. (2014). Adam: A Method for Stochastic Optimization *In*: *3rd International Conference on Learning Representations, ICLR 2015* [Online]., 1–15. Available from: http://arxiv.org/abs/1412.6980.

McCulloch W.S., Pitts W. (1943). A logical calculus of the ideas immanent in nervous activity, *The Bulletin of Mathematical Biophysics*, 5(4): 115–133.

O'Reilly G.J., Aristeidou S., Shahnazaryan D. (2024). On the application of neural networks to ground motion intensity and correlation modelling, *In*: *Proceedings of 18th world conference on earthquake engineering*. Milan, Italy.

Oyarzo-Vera C., Chouw N. (2008). Effect of earthquake duration and sequences of ground motions on structural responses *In*: *Proceedings of the 10th International Symposium on Structural Engineering for Young Experts, ISSEYE 2008*. Changsha, China, 1881–1886.

Raghunandan M., Liel A.B. (2013). Effect of ground motion duration on earthquake-induced structural collapse, *Structural Safety*, 41: 119–133.

Sarieddine M., Lin L. (2013). Investigation Correlations between Strong-motion Duration and Structural Damage *In*: *Structures Congress 2013* [Online]. Reston, VA: American Society of Civil Engineers, 2926–2936. Available from: http://ascelibrary.org/doi/10.1061/9780784412848.255.

Sousa L., Silva V., Marques M., Crowley H. (2016). On the treatment of uncertainties in the development of fragility functions for earthquake loss estimation of building portfolios, *Earthquake Engineering & Structural Dynamics*, 45(12): 1955–1976.

Spillatura A., Kohrangi M., Bazzurro P., Vamvatsikos D. (2021). Conditional spectrum record selection faithful to causative earthquake parameter distributions, *Earthquake Engineering & Structural Dynamics*, 50(10): 2653–2671.

Tarbali K., Bradley B.A., Baker J.W. (2023). Effect of near-fault directivity pulses on ground-motion intensity measure correlations from the NGA-West2 data set, *Earthquake Spectra*, 00(0).

Trifunac M.D., Brady A.G. (1975). A study on the duration of strong earthquake ground motion, *Bulletin of the Seismological Society of America*, 65(3): 581–626.